Journal of Applied Fluid Mechanics, Vol. 16, No. 4, pp. 618-633, 2023.
Available online at www.jafmonline.net, ISSN 1735-3572, EISSN 1735-3645.
https://doi.org/10.47176/jafm.16.04.1442

Turbulent One-dimensional Interfacial Scalar Transport: Statistical Random Square Waves Solution

H. E. Schulz [1, 2†] and F. A. L. Lavín [2, 3]

[1] *Hydro-Engineering Solutions (Hydro LLC), Auburn, Alabama, 36830, USA*
[2] *University of São Paulo (EESC-USP), São Carlos, São Paulo, 13566-590, Brazil*
[3] *Faculty of Engineering, University of Bio Bio,Concepción , Chile*

†*Corresponding Author Email: hschulz@hydro-engineering.net*

(Received July 16, 2022; accepted December 12, 2022)

ABSTRACT

In this study the mass transport through free turbulent liquid surfaces, or gas/liquid interfaces, is considered. The main direction of mass transfer is perpendicular to the interface, so that a one-dimensional point of view is followed. The equations for the interfacial gas/liquid transport are presented using the random square waves method (RSW), a statistical tool that models the fluctuations of physical variables as ideal signals. The method defines three statistical functions (partition, reduction, and superposition), related to fluctuations of concentration and velocity, which were introduced into the mass advection-diffusion equation generating a set of differential equations adequate for boundary layer problems. Solution profiles of the partition and reduction functions, and of turbulent fluxes across the boundary layer were obtained for transient situations. The solutions use Taylor series centered at the immersed border of the concentration boundary layer. For practical applications, the series were truncated and the coefficients were calculated in order to satisfy adequate physical conditions. The proposed procedure substitutes coefficients of the higher order parcels of the truncated series, enabling them to satisfy boundary conditions in the two borders of the domain of interest, which is the region of variation of the mass concentration. The theoretical profiles for concentration and turbulent fluxes close to the interface agree with measurements and predictions found in the literature.

Keywords: Statistical turbulence; Random square waves; Turbulent interfaces; Turbulence modelling; Gas-liquid interaction.

NOMENCLATURE

A	complementary reduction function
A_1	reference value of A at $z^*=1$
E	z position where $n=0$ and $dn/dz=0$
F	scalar field
f	scalar fluctuation
H	dimensionless coefficient
IJ	dimensionless turbulent flux
IJ_1	reference value of IJ at $z^*=1$
j	mass flux
K	transfer coefficient of F
K_L	mass transfer coefficient
Re	Reynolds number
Sc	Schmidt number
Sh	Sherwood number
m	partition function for velocity
n	partition function for scalar
t	time
U	x velocity
u	x velocity fluctuation
V	y velocity
v	y velocity fluctuation
W	z velocity
w	z velocity fluctuation
z	distance to interface (z=0)
z^*	z/E, normalized depth $0 \le z \le 1$
$z^\S$	z^*/δ^*, normalized depth $0 \le z^\S \le 1$
z_{BM}	normalized depth following [36]
a	reduction function, $a=1-A$
b	superposition function
d	concentration boundary layer thickness
δ^*	characteristic length $n(z^*=\delta^*)=0.01$
q	order of the statistical parameter
$1D$	one dimensional
Subscripts	
C	mass concentration
B	bulk liquid
S	surface
p	previous
n	next

1. INTRODUCTION

The exchange of scalar properties through free surfaces has become an intense research topic, a result of the many industrial applications and its vital role in biogeochemical cycles, involving biological aspects related to climate change (Gulliver 1991; Donelan *et al.* 2002; Wanninkhof *et al.* 2009). For example, engineers and scientists agree about the fundamental role of gas exchanges in water bodies to guarantee life. In natural environmental conditions, exchanges of gases between water and atmosphere occur along oceans, estuaries, and other natural liquid extensions, totalizing very large horizontal dimensions (around 3/4 of the Earth's surface). However, the atmosphere/water gas transfer process itself occurs mainly in the vertical direction, and through a very thin region (having a thickness of the order of millimeters) that characterizes the gas-liquid interface (Brumley 1984; Theofanous 1984; Brumley and Jirka 1987; Herlina and Jirka 2007). The studies in this thin region have inherent difficulties (Theofanous 1984; Jähne and Haussecker 1998), like the influence of turbulence, surface distortions, waves, generation of bubbles, drops, splashes and sprays, rain, contamination, among other aspects.

The gas transfer rate (or coefficient) K_L, usually quantified as $K_L=j/(C_S-C_B)$, where j is the mass flux, C_S and C_B are respectively the gas concentrations at the water surface and in the bulk liquid, depends on interactions between turbulence and molecular processes in the near-surface region (Hunt 1984; Brumley and Jirka 1988). Many different models using different tools were proposed to predict K_L (see, for example: Bennett and Rathbun 1971; Hunt 1984; Jorgensen and Gromiec 1989; Turney and Banerjee 2013), including conceptual models (Brumley and Jirka 1987), models based on surface divergence (McCready *et al.* 1986), empirical correlations, and direct numerical simulations (Magnaudet and Calmet 2006; Herlina and Wissink 2019), among others. Interfacial gas transfers may occur under a shared control between both the gaseous and the liquid phases. In general, the different models consider the liquid resistance as the dominant control mechanism for the mass flux of low soluble gases, which led Brumley and Jirka (1987) to present a structure in which the liquid in the near-surface region is composed by idealized hydrodynamic layers. Figure 1 shows these layers applied to both sides of the interface.

Taking a downwards vertical axis with origin at the interface, a *surface-influenced layer* (S) is firstly defined having a vertical thickness compatible with the integral length scale L_∞ obtained from turbulent velocity signals. The effects of the interface on the velocity due to the fluid viscosity are not significant outside of S (Bennett and Rathbun 1971; Brumley and Jirka 1987). Viscosity influenced layers are thus defined inside of S (vertical distances between the interface and the position S). For these viscous layers, the influence of the interface on large or small turbulence eddies are ideally considered, being the

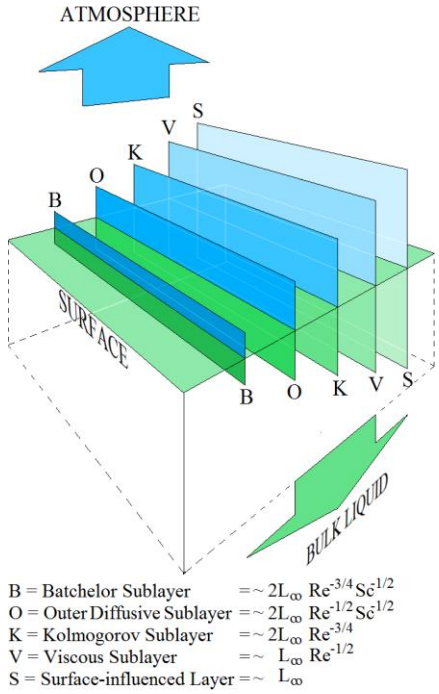

Fig. 1. BOKVS-BOKVS layers at gas-liquid interfaces. The heights of the vertical planes above and below the surface indicate thicknesses of the gaseous and liquid layers, respectively.

scale of the eddies determined from the turbulence spectrum. With this in mind, the vertical distance where larger eddies are affected by the interface is named the *viscous sublayer* (V), and the vertical distance where smaller eddies are affected by the interface is called the *Kolmogorov sublayer* (K).

Both viscous sublayers (V and K) may coexist with two mass transfer sublayers also subjected to turbulence, and which are defined taking into account the diffusion of the gas in the liquid while entering or leaving the liquid medium through the interface. The vertical distance from the interface where diffusive effects interact with the large eddies is named the *outer diffusive sublayer* (O), and similarly, the vertical distance from the interface where diffusive effects interact with small eddies is named the *Batchelor sublayer* (B). In Fig. 1 the relative position of the different layers depends on the Schmidt number *Sc*. The transfer control of highly soluble gases occurs in the gaseous phase (set of layers above the surface in Fig. 1). The present study considers lower soluble gases, controlled by the liquid phase, and the relative positions in Fig. 1 correspond to *Sc* numbers related to this case. Aiming to elucidate how the mass transfer process relates with the layers of Fig. 1, experimental studies were conducted in different sites (Chu and Jirka 1992; Tamburrino and Gulliver 2002; Schulz and Janzen 2009; McCorquodale and Munro 2017; Lacassagne *et al.* 2017a,b) proposing transport equations involving powers of Reynolds (Re) and Schmidt (Sc) numbers, various time and length scales, among other relevant parameters. The experimental data indicated that there is still a lack

of understanding about the underlying mechanisms of transfer and its relations with the defined layers, a situation that hinders the establishment of a more complete model for the gas transfer through interfaces. In this scenario it is interesting to remember the comment of Turney and Banerjee (2013) for the gas exchanges that "remain difficult to predict or simulate due to the wide range of length and time scales and lack of experimental observations of near-surface fluid velocity and gas concentrations". The B, O, K, V, S layers are among these length scales.

From the previous paragraphs, it is clear that the main gap existing between measurements and predictions relies on the value to be used for the gas transfer coefficient K_L in different agitation conditions. As mentioned, despite being possible to measure it experimentally, there is still no general correlation that allows explaining the effects of the different interferent phenomena on it. Among the many models that were proposed in the literature since the beginning of the 20th century, we mention the most referred, like the two films model described, for example, in Lewis and Whitman (1924); the penetration model of Higbie (1935), and the surface renewal model of Danckwerts (1951). Further, in the second half of the 20th century, the increasing use of river waters in a repetitive way while they flow to the ocean induced to study the self-aeration of the rivers. It helps to quantify the level of treatment of the wastewaters to be reintroduced into the rivers and which will be used again downstream. Empirical correlations were proposed, and so-called eddy models were suggested to encompass the influence of the turbulence (Lamont and Scott 1970, Luk and Lee 1986, for example). Large and small eddies were considered, and several proposals combining the different models may be found in the literature, like Toor and Marchello (1958).

Interfacial mass transfers induced under restricted conditions and in controlled devices (packed bed columns, for example, like shown by Flagiello *et al.* 2021) have empirical correlations for K_L that may produce acceptable predictions. However, this is not the case of natural water bodies, as commented in several experimental studies (e.g., Mackinnon *et al.* 2002). Empirical reaeration equations usually apply well only for the original set of data, being then used as approximate predictive tools only for very similar flow conditions. Predictive river quality tools like Qual 2E, for example, (EPA 1995) were built to consider different models for river stretches with different flow conditions. Even so, comparisons between measurements and predictions may present discrepancies (Cunha *et al*. 2011). Further, also semi-empirical and conceptual equations must have their coefficients and exponents adjusted for each new work condition, showing that the existing models still do not capture the entire phenomenon of interfacial mass transfer (Jähne 2020). These facts add practical limitations to the more conceptual scenario of the aforementioned multiplicity of scales (Turney and Banerjee 2013).

It is understood that the details of the evolution of the mean parameters in the very near surface region are essential for attaining adequate predictions of mass transfer. Many studies have been conducted to measure the mean mass concentration and mean velocities profiles in the sub-surface layer (Janzen 2006; Lacassagne *et al.* 2017a,b; Bongo *et al*. 2021). These studies are of paramount importance to link the conceptual models and theoretical assumptions to observed behaviors. In this sense, when considering the diffusive Fick law for continuous media in the turbulent case, the mass flux crossing the interface is proportional to the gradient (slope) of the mean concentration profile at that position. For slightly soluble gases it is generally assumed that the slope attains its maximum (in modulus) at the interface, so that the mass transfer models incorporate this assumption for any agitation condition. But it is still not possible to affirm that this is always the case. Results from optical techniques, like the Laser Induced Fluorescence (LIF), are linearized below the interface, suppressing unreal optical distortions (of course undesired) together with any eventual physical contribution to the concentration profile (a not quantified collateral effect of the linearization). As a consequence, a maximum slope is in fact "imposed" at the interface. The same effect occurs when adjusting predefined profiles having maximum slopes at the origin (surface). The description of the LIF optical technique, the linearization procedure and the use of semi-empirical profiles with unconditional maximum slope at the interface may be found, for example, in Herlina (2005), Herlina and Jirka (2004, 2007), among others. Considering the complete mass advection-diffusion equation, the mass flux at the interface is composed by the diffusive and the advective parcels, the last introduced as a mean product of velocity and concentration fluctuations (Hinze 1959) When applying the "Boussinesq mass flux equivalent hypothesis" (Hinze 1959), developed originally for momentum flux, it results that the turbulent parcel of the interfacial mass flux is also proportional to the gradient of the mean concentration at the interface. The previous paragraphs show that some usual procedures for turbulent flows concentrate effects of turbulence in a specific variable, which must then be correctly quantified. This is the case of the concentration profile, which derivative (slope) at the interface must be adequately defined in theoretical models, and precisely measured in experiments. Its modeling and measuring in the usually very thin superficial boundary layer emerge as fundamental to enable correct predictions of mass fluxes, and to substantiate the concepts built along the decades for the free shear transfer processes.

Statistical tools that allow this more detailed analysis are thus necessary. An alternative way to quantify turbulent scalar profiles (concentration profiles among them) and statistical parameters in boundary layer regions was searched by Schulz (1985) and Schulz and Schulz (1991), with the pioneering proposal to model the turbulent signals as square waves, a procedure named Random Square Waves method (RSW). The procedure followed in the proposal was to avoid the use of secondary models in the statistical problem of turbulence, like the Boussinesq hypothesis, when quantifying the mean

scalar profiles. The Boussinesq hypothesis evolved from the need to surpass the unknown average products of fluctuations in the statistical equations (Hinze 1959). As consequence, it introduces the so-called turbulent viscosities and diffusivities, which naturally need further models. The new conceptual point of view adopted in the RSW method was to take "turbulence" itself as the main initial "object" to be converted to a mathematical form, working with measured data of the scalar and vectorial variables under study (mass and velocity, in the present case). This is aligned with a more general formulation for turbulence obtained in this line of research and described by Schulz (2022), based on consolidated empirical results.

Theoretical improvements (Janzen 2006; Schulz *et al.* 2010; Lopes Jr 2012) gradually empowered the formulation, so that the statistical functions defined in the RSW method could be adequately used in the scalar advection-diffusion equation. Normalized analytical solutions were then obtained for the interfacial mass transport (Gonçalves and Schulz 2013; Gonçalves 2014; Schulz *et al*. 2018), firstly for the stationary regime (steady state) and a constant reduction function (a basic statistical element of the RSW method). In the sequence, for more general situations (transient flows with variable reduction function), the possibility of using Taylor series to obtain adequate concentration profiles and related statistical parameters was introduced (Lavín and Schulz 2019; Lavín 2020). Taylor series allow managing boundary conditions at different points of the domain of interest, like, for example, the contours of the region of variation of concentration. The present study shows the adequacy of this proposal, describing the main steps of the RSW method and the application of Taylor series. The results described in this study are more focused on the concentration profiles not subjected to implicit assumptions of maximum slopes at the air-water interface.

The solution for interfacial profiles is presented here as a nonlinear boundary value problem that is composed by three nonlinear differential equations subjected to six physically justified boundary conditions in two points of the domain of interest (contours). Three control parameters are relevant: 1) the modified Sherwood number, 2) the turbulent flux at a fixed position, and 3) the value of the mentioned reduction function at a fixed position. The method allows a more comprehensive view of interfacial mass transfer phenomena, and the relevant parameters for their quantification. The use of three control parameters is a novelty in the field of interfacial mass transfer, allowing obtaining profiles of normalized mass concentrations, turbulent mass fluxes, and reduction functions which follow the main aspects of measured profiles (comparisons with experimental data are shown along the text). As mentioned, the focus in the present study was to obtain the evolution of the mean statistical profiles close to the interface, evidencing details that are relevant for the quantification of the interfacial mass transfer, like the slope of the concentration gradient at this position.

2. STATISTICAL FUNCTIONS IN THE RSW METHOD

2.1 Basic Used Equations

The mass transfer in the subsurface region of a gas/liquid interface subjected to a velocity field $\boldsymbol{U} = (U, V, W)$ is generally quantified through the advection–diffusion equation, Eq. (1), which relates changes of the scalar field F to the movement of the liquid (velocity field) and to diffusion, expressed by the molecular diffusion coefficient D.

$$\frac{\partial F}{\partial t} + \boldsymbol{U} \cdot \nabla F = D \cdot \nabla^2 F \tag{1}$$

For turbulent liquids it is usual to adopt the Reynolds decomposition of the variables in the form $\boldsymbol{U} = (\bar{U} + u, \bar{V} + v, \bar{W} + w)$ and $F = \bar{F} + f$, and to apply a time average operator over the resulting equation. Uppercase and lowercase letters are instantaneous and fluctuating variables, respectively, and overbars indicate time averaged variables. Following Schulz *et al.* (2010), after using the Reynolds decomposition Eq. (1) was multiplied by $f^{\theta}=[F-\bar{F}]^{\theta}$, the scalar fluctuation f elevated to Θ and then averaged in time to obtain Eq. (2). $\overline{f^{\theta}}$ is named the θth moment of the concentration field, and Eq. (2) expresses its variation in time and space, also involving $\bar{F}$ (see Schulz *et al*. 2011; Gonçalves 2014).

For interfacial mass transfer, mean physical variables like concentration, velocity, and related statistical parameters vary mainly perpendicularly to the interface (z axis). A one-dimensional (1D) point of view was thus adopted, taking Eq. (2) for the z axis, and applying it in the concentration boundary layer below the interface. The free surface is shear-free; and the mean velocity in the liquid is zero. These conditions reproduce laboratory experiments done in water tanks, where only the turbulent movements are studied. Eq. (3) expresses the 1D case along z.

$$\begin{aligned}
&\overline{f^{\theta}}\frac{\partial \bar{F}}{\partial t} + \frac{1}{\theta+1}\frac{\partial \overline{f^{\theta+1}}}{\partial t} + \\
&\qquad + \overline{f^{\theta}}[(\bar{U},\bar{V},\bar{W}) \cdot \nabla \bar{F}] + \\
&+ \frac{1}{\theta+1}\left[(\bar{U},\bar{V},\bar{W}) \cdot \nabla \overline{f^{\theta+1}}\right] + \\
&+ \left(\overline{f^{\theta}u}, \overline{f^{\theta}v}, \overline{f^{\theta}w}\right) \cdot \nabla \bar{F} + \\
&+ \frac{1}{\theta+1}\nabla \cdot \left[\overline{(u,v,w)f^{\theta+1}}\right] = \\
&= D\left[\overline{f^{\theta}\nabla^2 \bar{F}} + \overline{f^{\theta}\nabla^2 f}\right]
\end{aligned} \tag{2}$$

$$\begin{aligned}
&\overline{f^{\theta}}\frac{\partial \bar{F}}{\partial t} + \frac{1}{\theta+1}\frac{\partial \overline{f^{\theta+1}}}{\partial t} + \overline{f^{\theta}w} \cdot \nabla \bar{F} + \\
&+ \frac{1}{\theta+1}\nabla \cdot \left[\overline{wf^{\theta+1}}\right] = \\
&= D\left[\overline{f^{\theta}}\frac{\partial^2 \bar{F}}{\partial z^2} + \overline{f^{\theta}\frac{\partial^2 f}{\partial z^2}}\right]
\end{aligned} \tag{3}$$

So far, the procedures are in the realm of the traditional statistical treatment of turbulence. From this point on, the procedures consider each statistical parameter of Eq. (3) as an object to be converted to the RSW format (Schulz *et al.* 2010, 2011). An *a*

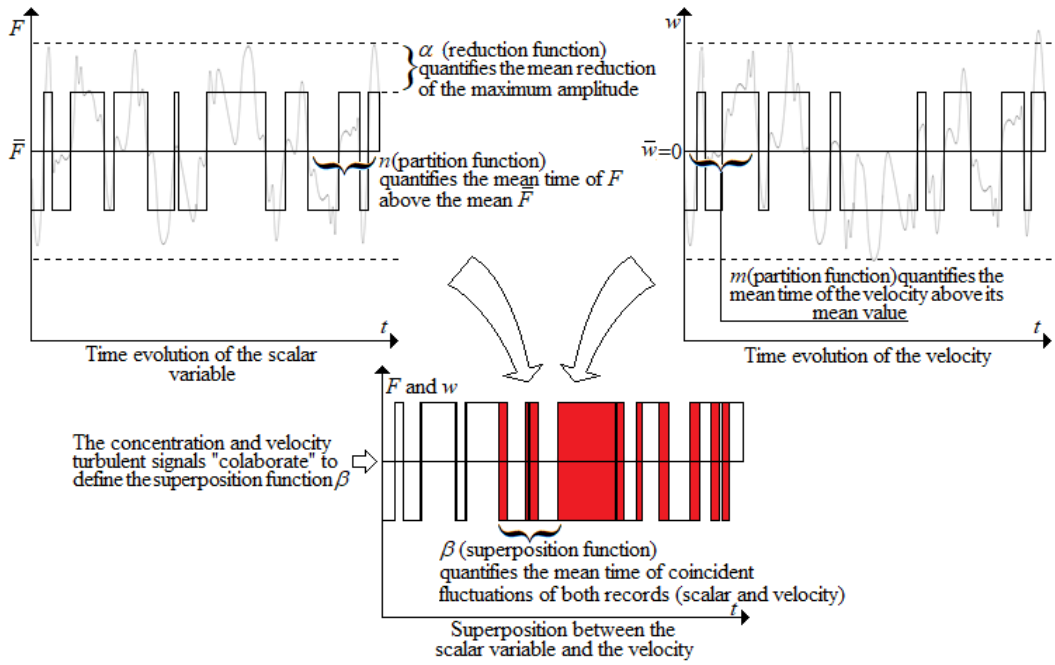

Fig. 2. The RSW method used to model concentration and velocity signals to square waves, keeping the mean values of the original signals. The proposed statistical functions have clear physical meanings

priori modeling of the turbulent signals is made, and proper functions with clear physical meaning are defined. Figure 2 sketches the *a priori* modeling of a mass concentration turbulent signal and a velocity turbulent signal into correspondent square waves, and shows the mentioned functions. Independent and "cooperative" functions (in the sense that they are defined considering both concentration and velocity signals) are needed, because the two signals have superposed parcels.

Aspects of the RSW functions of Fig. 2 are shown in Table 1 (see also Schulz *et al*. 2011), and the different statistical objects of Eq. (3) are listed in Table 2 in the RSW form. It can be observed in Table 2 that all objects of Eq. (3) are expressed using 4 of the 5 functions of Table 1, because the function m depends on the functions n and β, in the form m=1-(β+n-2βn). The RSW forms are bimodal versions of the statistical objects. The functions n and α reproduce the first two central statistical moments of the scalar mass concentration signal, and the functions m and $\sqrt{\overline{w^2}}$ are the first two central statistical moments of the velocity signal. With this arrangement, the 4 unknown functions need only 4 equations to generate a closed system, that is, the closure problem of statistical turbulence is surpassed using this scheme for scalar boundary layers. In the practical sense, the *a priori* definition of basic functions implies in using them in the whole set of statistical objects. As a very positive consequence, it avoids the *a posteriori* search of new physical principles to justify guesses for *a posteriori* defined variables, like the turbulent viscosities and diffusivities. Such additional variables are usually modelled following *ad hoc* proposals (see, for example, Rodi 2000). In table 2, F_p and F_n are the mass concentrations on both sides of the boundary layer (spatial domain of interest).

Table 1 Details of the RSW functions

Function	n	m	α	β	$\sqrt{\overline{w^2}}$
Dimension	ND	ND	ND	ND	m/s
Physical meaning	P	P	R	S	RMS
Maximum value	1	1	1	1	+/-not settled
Minimum value	0	0	0	0	+/- 0

ND: nondimensional; m=1-(β+n−2βn); P: partition; S: superposition; R: reduction; RMS: root mean square.

Table 2 Statistical objects in RSW form

Object	RSW representation	
$\bar{F}$	$nF_p + (1-n)F_n$	(4)
$\partial\bar{F}/\partial t$	$K(1-n)(F_p - F_n)$	(5)
$\overline{f^\theta}$	$n(1-n)(F_p - F_n)^\theta * \begin{bmatrix}(1-n)^{\theta-1} + \\ (-1)^\theta (n)^{\theta-1}\end{bmatrix}(1-\alpha)^\theta$	(6)
$\overline{f^\theta w}$	$\sqrt{\dfrac{n(1-n)}{n(1-n)+\dfrac{\beta(1-\beta)}{(2\beta-1)^2}}} * \begin{bmatrix}(1-n)^\theta - \\ (-n)^\theta\end{bmatrix}\dfrac{\sqrt{\overline{\omega^2}\ \overline{f^{2\theta}}}}{\sqrt{\begin{bmatrix}(1-n)^{2\theta-1} + \\ (-1)^{2\theta}(n)^{2\theta-1}\end{bmatrix}}}$	(7)
$\overline{f^\theta \dfrac{\partial^2 f}{\partial z^2}}$	$n(1-n)(1-\alpha)^\theta (F_p - F_n)^{\theta+1} \cdot \begin{bmatrix}\dfrac{(1-n)^{\theta-1}\partial^2[(1-n)(1-\alpha)]}{\partial z^2} \\ +(-n)^\theta \dfrac{\partial^2[-n(1-\alpha)]}{\partial z^2}\end{bmatrix}$	(8)

In Table 2 "p" denotes "previous" to the domain, being the interface in this study; and "n" denotes

"next" to the domain, being the bulk liquid in this study. F_p is defined by environmental conditions (pressure and temperature, for example), mainly constant along the experiments.

Figure 2 and Table 1 show the partition functions n and m; the reduction function α; the superposition function β (being m, n, and β related), and the RMS of the velocity, $\sqrt{\overline{\omega^2}}$. These are the only functions needed for 1D scalar transfers. It is possible to represent the statistical objects using different schemes (Janzen 2006). The bimodal RSW scheme models the turbulent signals as shown in Fig. 2, and the use of Taylor series to obtain solutions of the concentration profiles and of the main interferent variables represents a novelty in this field of study. Other ways of modelling the original turbulent signals can be proposed, a theme that is not developed in the present study.

2.2 RSW Equation

Applying the RSW objects of Table 2 into Eq. (3), and taking θ=1 (first statistical moment), Eq. (9) is obtained. It is the usual one-dimensional advection diffusion equation in RSW format. For $\theta \geq 2$, the subsequent RSW moments are given by Eq. (10).

$$1-n=\frac{1}{Sh}\frac{d^2n}{dz^{*2}}-\frac{dIJ}{dz^*} \tag{9}$$

$Sh=\{KE^2\}/D$ is a modified Sherwood number, being $K=K_L/E$, and $z^*=z/E$ the normalized distance to the interface. E is the characteristic length that limits the domain of interest (region of variation of concentration, see Fig. 3).

$$\begin{aligned}&-n(1-n)\begin{bmatrix}(1-n)^{\theta-1}+\\(-1)^{\theta}(n)^{\theta-1}\end{bmatrix}A^{\theta}\\&+n(1-n)^2\left[(1-n)^{\theta-2}\right.\\&\left.+(-1)^{\theta-1}(n)^{\theta-2}\right]A^{\theta-1}\\&IJ\left[(1-n)^{\theta-1}-(-n)^{\theta-1}\right]A^{\theta-2}\frac{dn}{dz^*}+\\&\frac{1}{\theta}\frac{d}{dz^*}\left\{IJ\left[(1-n)^{\theta}-(-n)^{\theta}\right]A^{\theta-1}\right\}=\\&\frac{n(1-n)A^{\theta-1}}{Sh}\left[\begin{array}{c}\left[\begin{array}{c}(1-n)^{\theta-2}+\\(-1)^{\theta-1}\cdot n^{\theta-2}\end{array}\right]\frac{d^2n}{dz^{*2}}+\\\frac{(1-n)^{\theta-2}d^2[(1-n)A]}{dz^{*2}}\\+\frac{(-n)^{\theta-2}d^2[(-n)A]}{dz^{*2}}\end{array}\right]\end{aligned} \tag{10}$$

IJ is the dimensionless turbulent flux, which is related to the superposition function β and to the RMS velocity $\sqrt{\overline{w^2}}$ through Eq. (11).

$$IJ=\frac{n(1-n)A\left(\frac{\sqrt{\overline{w^2}}}{KE}\right)}{\sqrt{n(1-n)+\frac{\beta(1-\beta)}{(2\beta-1)^2}}} \tag{11}$$

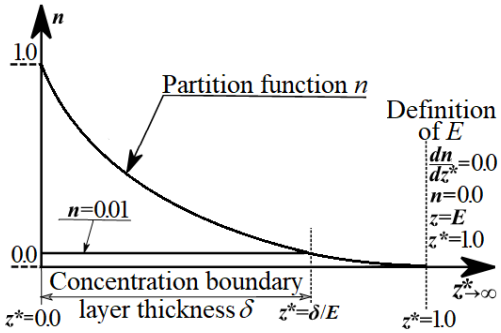

Fig. 3. Boundary conditions that define *E* and *δ*, conditioned by the partition function *n*.

Equation 10 shows that each moment (θ=2,...,∞) generates one differential equation. A set of infinite equations is thus possible, resembling the closure problem of turbulence. However, as already mentioned, because only four unknown functions are used (n, α_f, β and $\sqrt{\overline{w^2}}$), only four equations are needed. This finite possibility is improved further because the variables β and $\sqrt{\overline{w^2}}$ appear always connected through IJ (see Eq. 11). It is then possible to consider IJ an unknown variable, and to use only θ=1, 2, and 3, that is, there are only three function to determine (n, α_f, and IJ). For θ=2 and 3 Eqs. (12), and (13) are then obtained, respectively.

$$\begin{aligned}&-n(1-n)A^2+IJ\frac{dn}{dz^*}+\frac{d[IJA(1-2n)]}{2dz^*}\\&=\frac{1}{Sh}n(1-n)A\frac{d^2[(1-2n)A]}{dz^{*2}}\end{aligned} \tag{12}$$

$$\begin{aligned}&n(1-\mathrm{n})A^2\{-(1-2\mathrm{n})A+1-n\}+\\&\frac{(1-2\mathrm{n})IJAd\mathrm{n}}{dz^*}\\&+\frac{d[IJA^2(1-3n+3\mathrm{n}^2)]}{3dz^*}\\&=\frac{n(1-n)\mathrm{A}^2}{Sh}\left[\begin{array}{c}\{1-A(1-2n)\}\frac{d^2n}{dz^{*2}}+\\\{1-2n+2n^2\}\frac{d^2A}{dz^{*2}}+\\2\{2n-1\}\frac{dn}{dz^*}\frac{dA}{dz^*}\end{array}\right]\end{aligned} \tag{13}$$

Eqs. (9), (12) and (13) form a closed set that, with proper boundary conditions, is enough to obtain the one-dimensional evolution of scalar variables and related functions. It is interesting to note that Eq. (11), although having being used to generate the three set of equations, is not a part of this set. This fact is used in the sequence to relax the value of IJ at the boundary z^*=1, which may then assume nonzero values without imposing the condition $\beta(z^*=1)=0$, which would generate an indetermination.

The closed set of three equations was obtained by defining the three functions to be calculated by the equations, and not by imposing *ad hoc* models.

2.3 Boundary Conditions

The interfacial turbulent mass transfer is thus converted to a nonlinear boundary value problem, with values of functions and derivatives to be given at several points of the domain of interest (borders of the region of variation of the mass concentration). The six boundary conditions for the three second order differential equations are:

i) n=1 at z^*=0.0 (the normalization leads to the unitary n at the interface).

ii) A=0 at z^*=0.0 (diffusive effects are dominant close to the interface).

iii) IJ=0 at z^*=0.0 (diffusive effects are dominant close to the interface).

iv) dIJ/dz^*=0 at z^*=0.0 (turbulence is damped when approaching the surface, not only at the surface).

v) n=0 at z^*=1.0 (for $z \geq E$ or $z^* \geq 1.0$ the condition of the bulk liquid prevails).

vi) dn/dz^*=0 at z^*=1.0 (for $z^* \geq 1.0$ no variations of n occur along z in the bulk liquid and its boundary).

These are physically justified boundary conditions assumed for the present study. Further studies on the theme may consider different positions along z^*, involving other assumptions, related to the situation under study. Conditions v) and vi) occur at z^*=1 (or z=E), and define the immersed border of the region of variation of concentration. Because n=0 in this position, the length E is always longer than the length δ of the boundary layer, conditionally defined as the position where the normalized concentration profile attains the value n=0.01 (Fig. 3). The profile n thus allows obtaining the length of the boundary layer δ.

2.4 The Solution Through Taylor Series

The center of attention of the study was the normalized concentration profile, or partition function, n. The solution was obtained by applying Taylor series centered at the position z^*=1.0, where two boundary conditions for n are known. The Taylor series were built for n, A, and IJ. The definition of IJ of Eq. (11). was relaxed by using truncated series, being solved as part of the set given by Eqs. (9), (12) and (13) Coefficients of Taylor series involve successive derivatives applied at the center of the expansion (z^*=1 in the present case), which may be viewed as an "infinite number" of boundary conditions at this position. An algorithm to generate the successive derivatives (boundary conditions) was elaborated in symbolic MATLAB®, facilitating this task, as described by Lavín (2020). The coefficients of the series were calculated sequentially. Firstly, by applying conditions v) and vi) into Eqs. (12) and (13) generates the system of Eqs. (14), which solution for $A_{z^*=1} \neq 0$ and $IJ_{z^*=1} \neq 0$ (relaxing $IJ_{z^*=1}$) furnishes $dIJ/dz^*_{z^*=1}=0$ and $dA/dz^*_{z^*=1} = 0$.

$$\begin{cases} A_{z*=1} \cdot \dfrac{dIJ}{dz^*}_{z*=1} + IJ_{z*=1} \cdot \dfrac{dA}{dz^*}_{z*=1} = 0 \\ A_{z*=1} \cdot \dfrac{dIJ}{dz^*}_{z*=1} + 2IJ_{z*=1} \cdot \dfrac{dA}{dz^*}_{z*=1} = 0 \end{cases} \tag{14}$$

In the sequence, by applying $dIJ/dz^*_{z^*=1}=0$ into Eq. (9) furnishes $d^2n/dz^{*2}_{z^*=1}=Sh$. The further step consists in obtaining the derivatives of Eqs. (9), (12), and (13), generating higher order derivatives of the auxiliary functions, and reapplying the already known boundary conditions at z^*=1. In successive similar steps, higher order boundary conditions are obtained. For example, the set of second derivatives of A and IJ at z^*=1 is:

$$\begin{cases} \dfrac{d^2A}{dz^{*2}}_{z*=1} = -Sh \cdot (1 - A_{z*=1}) \\ \dfrac{d^2IJ}{dz^{*2}}_{z*=1} = -\dfrac{IJ_{z*=1}}{A_{z*=1}} Sh \cdot (1 - A_{z*=1}) \end{cases} \tag{15}$$

The whole set of Taylor series coefficients (boundary conditions at z^*=1) depends only on the three parameters, $A_{z^*=1}$, $IJ_{z^*=1}$, and Sh. For simplification of notation, the substitutions A_1=$A_{z^*=1}$, and IJ_1=$IJ_{z^*=1}$ are used in the sequence of the text. The symbolic MATLAB® code described by Lavín (2020) furnishes the vector [$n^{(p)}$, $A^{(p)}$, $IJ^{(p)}$], where p indicates the pth order derivative.

3. Applying the Taylor Series

3.1 The Calculation Domain $0 \leq z^* \leq 1$

The nonlinear boundary value problem needs to obey the physically justified boundary conditions at z^*=0, even being centered, in the present study, at z^*=1.0. The region $0 \leq z^* \leq 1.0$ is the domain of calculation of this study, and the series for n, A, and IJ need to be adequately truncated and subjected to the boundary conditions at z^*=0. This is accomplished through substitution of coefficients of the truncated series (replacing boundary conditions that change those coefficients).

3.2 Truncated Series and Substitution of Coefficients

Taking $N(z^*)$ as a common representation of any of the functions $n(z^*)$, $A(z^*)$, and $IJ(z^*)$, the related truncated Taylor series is written as:

$$\begin{aligned} N(z*) = N_{z^*=1} + \frac{(z^*-1)}{1!}\frac{dN}{dz^*}_{z^*=1} + \\ \frac{(z^*-1)^2}{2!}\frac{d^2N}{dz^{*2}}_{z^*=1} + \\ \frac{(z^*-1)^3}{3!}\frac{d^3n}{dz^{*3}}_{z^*=1} + \\ \ldots + \frac{(z^*-1)^t}{(t+1)!}\frac{d^tn}{dz^{*t}}_{z^*=1} + \cdots = \\ N_0 + N_1(z^*-1) + N_2(z^*-1)^2 + \cdots \\ + N_t(z^*-1)^t + \cdots \end{aligned} \tag{16}$$

The derivatives calculated at z^*=1 (boundary conditions) are present in the coefficients of the series. Further, the highest order coefficients of the already truncated series are recalculated (replaced) to guarantee the boundary conditions at z^*=0. In this sense, Eq. (16) has t known derivatives and t+1 coefficients. The (t+1)th coefficient (denoted as N_t) is

recalculated applying one of the boundary conditions at $z^*=0$ into the truncated series, and obtaining N_t as:

$$N_t = \frac{N_{z*=0} - \sum_{i=0}^{t-1} N_i\,(-1)^i}{(-1)^t} \tag{17}$$

The series for n and A use directly this procedure, with the previous boundary conditions "i" for n, and "ii" for A. However, the normalized turbulent flux IJ is subjected to the ***two*** boundary conditions "iii" and "iv" at $z^*=0$. In this case two coefficients N_{t-1} and N_t are recalculated for the truncated Eq. (16) and its derivative, generating a system of two equations and two unknowns (N_{t-1} and N_t). The solution of the system is given by Eqs. (17) and (18).

$$N_{t-1} = \frac{\sum_{i=1}^{t-2} N_i\, i(-1)^{i-1} - t\left[N_0 - \sum_{i=0}^{t-2} N_i\,(-1)^i\right]}{(-1)^{t-2}} \tag{18}$$

Note that:1) the Taylor series are centered at $z^*=1$, so that the coefficients given by Eqs. (17) and (18) involve A_1 and Φ_1, boundary values at $z^*=1$; 2) the Taylor series are applied at $z^*=0$, so that the coefficients also involve boundary values of n, A, and IJ at $z^*=0$. Further, the coefficients depend on the physical characteristics that define $Sh=(KE^2)/D$, composed by molecular and turbulent factors. As example, Table 3 presents the seven first coefficients (derivatives) of the Taylor series for n. Calculations were performed in the present study using 24 coefficients for the n and A profiles, and with 25 coefficients for the IJ profiles.

4. EXPERIMENTAL LITERATURE PROFILES AND CALCULATED PROFILES

In this section, literature examples are compared with calculations of the RSW method. Because there are three unknowns n, A, and IJ in the system of equations, the dependence of each unknown on the control parameters A_1, IJ_1 and Sh is discussed. The literature data show that adequate values of the control parameters generate profiles in the range of the observed behaviors.

4.1 Profiles of the Partition Function *n*

In the literature of interfacial air-water mass transfer in laminar flows the concentration profile for slightly soluble gases at the liquid phase may have the form shown in Fig. 4a, adapted from Boyadjiev and Mitev (1977). The figure shows the z_{BM} normalized distance to the surface as defined by Boyadijev and Mitev (1977). As seen, the concentration profile may have a smaller slope or gradient at the interface (in absolute value) than at deeper segments of the profile. Mathematically it is expressed as

$$\left|\frac{dn}{dz}\right|_{z=0} < \left|\frac{dn}{dz}\right|_{0<z<bulk\ liquid\ region} \tag{19a}$$

However, for turbulent flows it is generally accepted that the maximum slope (in absolute value) occurs at the interface (z_{BM} =0). Mathematically it is then accepted that

$$\left|\frac{dn}{dz}\right|_{z=0} > \left|\frac{dn}{dz}\right|_{0<z<bulk\ liquid\ region} \tag{19b}$$

Taking this into consideration, observed smaller local slopes in turbulent cases are justified as optical distortions of the measurement techniques (Jähne and Haussecker 1998; Herlina and Jirka 2004; Herlina 2005; Friedl 2013), which are then corrected for example by extending a straight line from the point of the profile having maximum slope until the surface, and substituting this segment of the original profile by the line. A second used procedure is to

Table 3 *p*-th derivative of the partition function *n* at *z*=1*

Order p	p-th derivative
0	0
1	0
2	Sh
3	$-\frac{IJ_1}{A_1}\ Sh^2(1-A_1)$
4	$\left(\frac{IJ_1}{A_1}\right)^2 Sh^3(1-A_1)^2 - Sh^2(3A_1+2)$
5	$-\left(\frac{IJ_1}{A_1}\right)^3 Sh^4(1-A_1)^3 - 2\frac{IJ_1}{A_1}\ Sh^3(1-A_1)(1-9A_1) - 3\frac{A_1}{IJ_1}Sh^2(1-3A_1)$
6	$\left(\frac{IJ_1}{A_1}\right)^4 \begin{bmatrix} Sh^5 * \\ *\,(1-A_1)^4 \end{bmatrix} + \left(\frac{IJ_1}{A_1}\right)^2 \begin{bmatrix} Sh^4 * \\ *\,(1-A_1)^2 * \\ *\,(61A_1-20) \end{bmatrix} + \begin{bmatrix} Sh^3 * \\ \begin{pmatrix} 156{A_1}^2 \\ -124A_1 \\ +199 \end{pmatrix} \end{bmatrix} - 18\left(\frac{A_1}{IJ_1}\right)^2 \begin{bmatrix} Sh^2 * \\ *\,(1-3A_1) \end{bmatrix}$
7	$-\left(\frac{IJ_1}{A_1}\right)^5 \begin{bmatrix} Sh^6 * \\ *\,(1-A_1)^5 \end{bmatrix} + \left(\frac{IJ_1}{A_1}\right)^3 \begin{bmatrix} Sh^5 * \\ *\,(1-A_1)^3 * \\ *\,(17-41A_1) \end{bmatrix} + \left(\frac{IJ_1}{A_1}\right) \begin{bmatrix} Sh^4 * \\ * \begin{pmatrix} 1445{A_1}^3 \\ -2624{A_1}^2 \\ +2814A_1 \\ -1635 \end{pmatrix} \end{bmatrix} - \left(\frac{A_1}{IJ_1}\right) \begin{bmatrix} Sh^3 * \\ \begin{pmatrix} 78{A_1}^2 \\ +2101A_1 \\ +191 \end{pmatrix} \end{bmatrix} - 180\left(\frac{A_1}{IJ_1}\right)^3 \begin{bmatrix} Sh^2 * \\ *\,(1-3A_1) \end{bmatrix}$

adjust, through least square methods, a semi-empirical model with an *a priori* defined maximum slope at the interface. Several functions can be adjusted to measured data, as shown by Friedl (2013), and Schulz and Gonçalves (2015), being the exponential function the most usual. Undoubtedly, profiles for turbulent conditions tend to be steeper than laminar profiles. But the possibility of having a turbulent concentration profile that evolves from a smaller slope to a steeper slope from the interface to a subsurface position (in the sense of Eq. 19a) is still an open question. If smaller slopes are possible at $z^*=0$, then to impose a straight line or an *a priori* function with the highest gradient at $z^*=0$ may camouflage the effect of turbulence in different scalar transfer events, pointing to the importance of studies on this theme.

Literature results use different characteristic lengths to normalize the z distance, shortly described or indicated in this study when needed. Many data are normalized with the traditional boundary layer thickness δ (position for n=0.01). When needed for comparisons, this procedure was also followed here, being the normalized z axis then presented as $z^{\S}=z/\delta$.

Fig. 4b shows the envelope region of experimental data obtained by Friedl (2013). The normalized axis z/f involves a characteristic length f obtained by the mentioned author from best adjusted functions.

Close to n=1 (or z/f=0) the gray envelope shows a trend to smaller slopes (Eq. 19a), and the data split in two functions at larger distances from the surface, depending on the induced or imposed agitation intensity. The existence of different functions that describe n profiles for different turbulent conditions was also discussed by Schulz and Gonçalves (2015), who showed that several solutions are obtained from the single basic governing differential Eq. (20), where H is a nondimensional integration constant.

$$\frac{dn}{dz^*} = H\left(\frac{1+\theta_2}{1-\theta_2}\right)^{\frac{\theta_1}{2}}\left[\left(\frac{1-\frac{\theta_3 n}{1+\theta_2}}{1+\frac{\theta_3 n}{1-\theta_2}}\right)^{\frac{\theta_1}{2}} - 1\right]$$
$$\theta_1 = 2(1-A)/\left(A\sqrt{4A^2+1}\right)$$
$$\theta_2 = (2A-1)/\sqrt{4A^2+1}$$
$$\theta_3 = 4A/\sqrt{4A^2+1} \qquad (20)$$

The solutions express explicitly z^* as a function of n (and not n as function of z^*). For example, the pair θ_1=2, H=2.6980 and the pair θ_1=4, H=6.6779 produced Eqs. (21a) and (21b), respectively.

$$z^* = -0.20470[n + 0.84587\ln(n) - 1] \qquad (21a)$$

$$z^* = -0.19690\begin{bmatrix} 068076\ln(n) - \\ 5.7913\ln(2.509-n) \\ -n + 3.3517 \end{bmatrix} \qquad (21b)$$

The procedures to define the values of A and H are shown in Schulz and Gonçalves (2015). The different functions obtained from the integration of Eq. (20) for different turbulent conditions give support to experimental results like Friedl (2013).

Figure 4c shows profiles of n obtained for transient regime and variable A (present study) together with the profiles obtained by Schulz *et al*. (2018) for steady state and constant A. The parameters A_1, IJ_1, Sh were varied in such a way to produce results that follow independently Eq. (19a) or Eq. (19b). The present profiles were obtained for A_1=0.76, IJ_1= 7, and Sh=0.56, and for A_1=0.80, IJ_1= 5, and Sh=0.01. It was observed that Sh has an upper limit to obtain adequate profiles, and that this limit depends on IJ_1 and A_1. Above this limit the profiles of n, A, and/or IJ show nonrealistic values (for example n > 1, A>1 and/or IJ<0 for 0≤ z^* ≤1). Care was taken to use realistic combinations of A_1, IJ_1, and Sh. Profiles of n obtained by Schulz *et al*. (2018) for A=0.43099 and

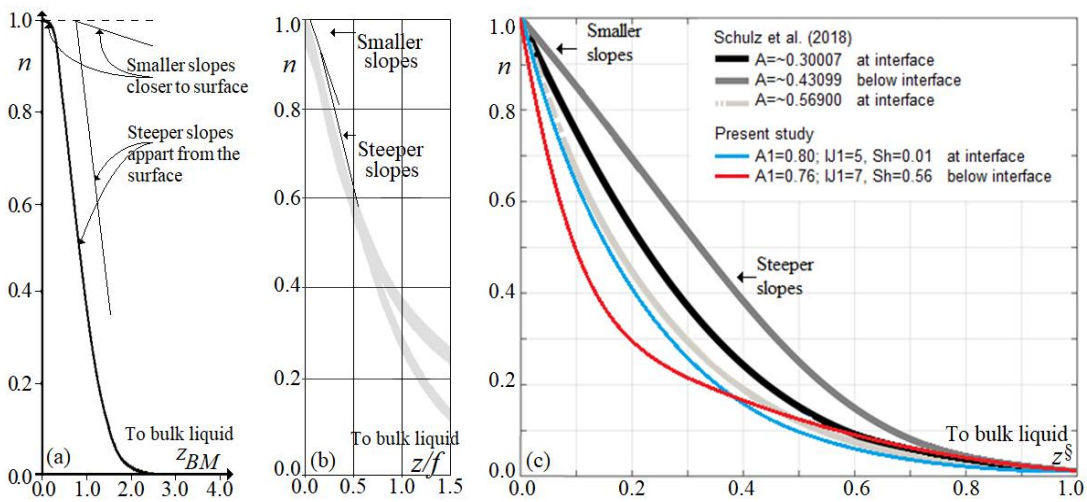

Fig. 4. *n* profiles: a) Laminar flows adapted from Boyadjiev and Mitev (1977); b) Envelope of measured data of Friedl (2013), turbulent flows; c) RSW results: black and gray tones from literature for steady state and constant *A*. Colored red and blue profiles are results of the present study.

here for A_1=0.76, IJ_1= 7, and *Sh*=0.56 followed Eq. (19a), that is, smaller slopes at the interface, similarly to the proposal of Boyadijev and Mitev (1977) for laminar flows. Further, profiles obtained by Schulz *et al.* (2018) for *A*=0.30007 and 0.56900, and here for A_1=0.80, IJ_1= 5, and *Sh*=0.01 followed Eq. (19b), the most usual observation and assumption encountered in the literature. Additionally, the profiles of Schulz *et al.* (2018) for *A*=0.56900, and of this study for A_1=0.80, IJ_1= 5, and *Sh*=0.01 showed similar behaviors.

Figure 5 allows observing in detail that the curve for A_1=0.76, IJ_1= 7, and *Sh*=0.56 follows Eq. (19a). Figures 4 and 5 show that different behaviors of d*n*/d*z** at the interface are obtained both for the stationary condition of the scalar field with constant *A* and for the non-stationary condition with variable *A*. The slope depends on the agitation of the liquid and the physical properties of the fluids into contact (gas and liquid).

In the practical sense, it remains to determine how to combine A_1, IJ_1, and *Sh* as design parameters, that is, to use them adequately to obtain real profiles and mass fluxes. Because maximum or lower slopes of *n* may occur at the interface, measured lower values of the literature may be reproducing part of the physical reality, so that optical distortions may be only partly affecting the measurements. This shows that further studies on the RSW method together with experiments will be very welcomed. Figures 6a, b compare RSW and measured profiles of *n*. The theoretical curves are obtained by imposing *Sh* as known variable. But for the measured data *Sh* depends on the used length scale, because *E* remains unknown from the observations. The hachured dark cloud shows measured data of Janzen (2006) also used by Janzen *et al.* (2010 a, b) superposing the light gray cloud of the profiles of Fig. 4c. Janzen *et al.* (2010a, b) applied seven models to observed interfacial gas transfer data allowing obtaining, for the so-called film model, mean values of δ=1.15.10^{-3}m, K_L=2.16.10^{-6} m/s, with *D*=2.47.10^{-9} m^2/s. Using the boundary layer thickness δ in place of *E* led to *Sh*≅1.0. Further, the so-called diffusive layer obtained by Janzen *et al.* (2010a, b) was about 28.7% of δ, which, maintaining unaltered the other variables, also reduces *Sh* to about 0.287. Asano (2006) reviewed the definitions of *Sh* pointing to their differences and dependence on arbitrary length scales, proposing a new form based on the molar flux. In the present study, being aware of the indefinite length scale, the *Sh* of observed data is not specified, and references to *Sh*≅1.0 (for δ) and *Sh*≅0.287 (for the diffusive layer) serve as examples. The theoretical range was restricted to 0.01<*Sh*<0.6. The RSW curves of Fig.e 6a were obtained for A_1=0.6, IJ_1=5, and *Sh* varying from 0.01 to 0.56, the last value being the limiting value for this union of control parameters. The obtained *n* profiles show a "down-and-up" behavior with *Sh*. In other words, the profiles of *n* have not a monotonic behavior with *Sh*. This aspect is also observed in Fig. 6b, obtained for A_1=0.6 and IJ_1=5, and for which the limiting value of *Sh* is 0.49. In this case, the profile of *Sh*=0.49 is very close to the measured values of Janzen (2006), being this value of *Sh* in the range of the mentioned reference values of 0.1 and 0.287. The behavior of doubling the *n* profiles observed in the data of Fig. 4b of Friedl (2013) is also observed in Fig. 6a, b for the different agitation conditions expressed by the control parameters. Figure 6b, for example, shows it clearly for the *Sh* values of 0.10 and 0.30, and for the *Sh* values of 0.01 and 0.49. In addition, *Sh*=0.49 leads to a maximum derivative of *n* (in modulus) for $z^{\S}\neq 0$, better detailed in the discussion of Fig. 14.

In view of the indefinite length scale for *Sh*, the experimental and theoretical profiles must still be compared to attain a best adjustment condition. The

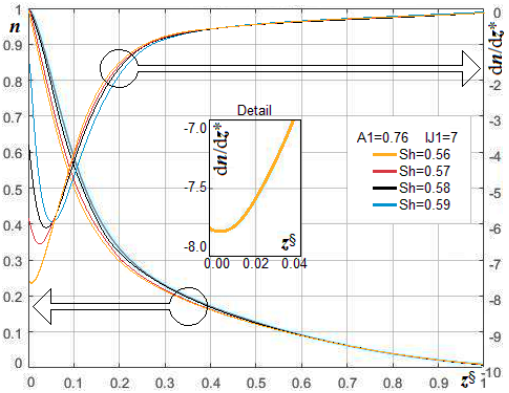

Fig. 5. Curves *n* and d*n*/d*z for A_1=0.76, IJ_1 =7, variable *Sh* with maximum slopes of *n* for $z^{\S}\neq 0$.**

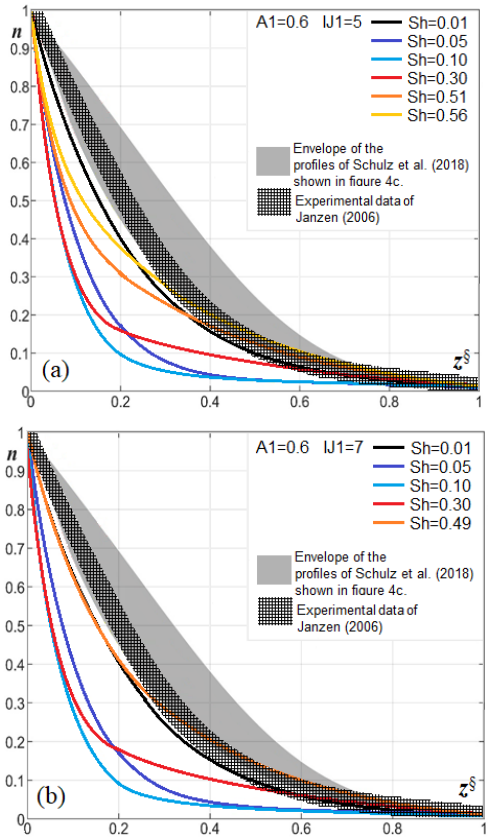

Fig. 6. *n* curves for A_1=0.6; a) IJ_1 =5, variable *Sh*; b) IJ_1 = 7, and *Sh*=0.49 close to the observations.

question of the length scale can then be studied in detail, a procedure needed to generate design tools, and not followed in the present study because of the present lack of specific experimental data.

Additionally, the present discussion shows that procedures that "impose" the whole slope reduction of n at z→0.0 as being optical distortions may need a refining, which may depend on the level of turbulence of the interface. Similarly, adjustments may be necessary for numerical codes that also impose the maximum slope of n to always occur at the interface.

4.2 Profiles of the Complementary Reduction Function A=1-α

As aforementioned, the quantification of the partition function, or the normalized concentration profile n, was the part of the problem that concentrated most of the attention of the present study. It is however evident, from the formulation, that the concentration profile depends on the other variables of the RSW method, and on physical properties of the gaseous and liquid phases. In this sense, the profiles of the interferent variables are also important, and the present discussion shows aspects of these profiles that can be considered in future studies to improve the applicability of the method.

Fig. joins observed and calculated A profiles for different values of A_1, IJ_1 and Sh. The experimental data of the light brown profiles were adapted from Janzen (2006), and Schulz and Janzen (2009), and involve several agitation levels. The mentioned authors normalized the measured axis z with the value z= $\delta_{c'}$ of the peak of the profile of the RMS concentration fluctuations $c' = \sqrt{A\,n(1-n)}$, which was also used here to allow comparisons. The RSW profiles were obtained for different values of the control parameters, as shown in the figure.

For A_1=0.6, IJ_1=5, and Sh= 0.56 the obtained profile follows the "growth and fall" experimental behavior, a good result that indicates that the RSW method may produce a broad range of forms of functions. It

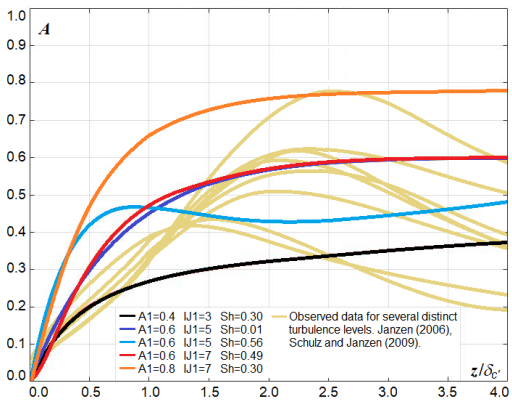

Fig. 7. RSW *A*-profiles for several sets of parameters, and observed *A*-profiles for various agitation conditions

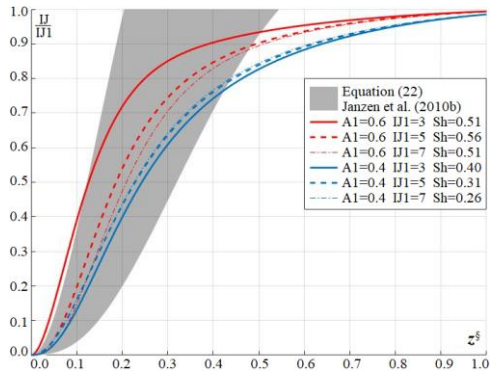

Fig. 8. *IJ*-profiles for IJ_1=5, A_1=0.4 and0.6. Gray represents Eq. (22) from Janzen *et al.* (2010b).

is observed that the combination A_1=0.6, IJ_1=7, and Sh= 0.49, which produced the n profile close to the measured data (Fig. 6b) produces a profile of A that is well located in the measurement region. The comparison of Fig. 7 between experiments and theoretical calculations shows that both experimental and additional RSW theoretical studies will be welcomed to better set the conditions that affect the molecular and turbulent contributions in the quantification of A. It must be mentioned that, in the present stage of the studies, experimental detailed A or α profiles are still rare in the literature.

4.3 Profiles of the Turbulent Flux *IJ*

The evolution of the variables that interfere in the formation of the normalized concentration profile n also involves the RSW turbulent flux. Different combinations of IJ_1, Sh, and A_1 were tested and are shown in Fig. 8. For comparison with previous results, they are plotted together with the predictions of Eq. (22) proposed by Janzen *et al*. (2010b), and represented by the gray cloud. The cloud was obtained for 2≤a≤3, and κ=4 in Eq. (22), following the indications of Janzen *et al.* (2010b). For the calculations of the Taylor series A_1 assumed the values 0.4 and 0.6, J_1 assumed the values 5 and 7, for variable Sh.

$$\frac{IJ}{IJ_1} = \frac{\left(\frac{\kappa \cdot z^{\S}}{a}\right)^{a} e^{-\kappa \cdot z^{\S}+a}}{\left[\left(\frac{\kappa \cdot z^{\S}}{a}\right)^{a} e^{-\kappa \cdot z^{\S}+a}\right]_{z^{\S}=1}} \tag{22}$$

Figure 8 shows that the different RSW results have a smooth increasing with $z^{\S}$, and that the profiles for A_1=0.6 furnished higher values than those for A_1=0.4 in the range 0.01 ⩽ Sh <0.3, although for the lower values of Sh=0.01 and 0.05 the differences are not visible in this graph (indicated as superposed profiles). For $z^{\S}$ →0 the RSW profiles and the gray cloud show very similar behaviors, which may be indicating a general trend of the phenomenon for $z^{\S}$→0, following Eq. (22) for z^{+}→0 (Janzen *et al.* 2010b). On the other hand, for larger distances to the interface Eq. (22) predicts a peak of IJ/IJ_1 > 1 for

$z^{\S}$<1.0. Peaks were in fact measured by Janzen *et al.* (2010b), not necessarily for $z^{\S}$<1.0, but showing that this behavior may be expected for interfacial transfer phenomena. In the present analysis IJ_1 is the reference value at z^*=1, where the value dIJ /dz^*=0 is the solution of Eqs. (14). This null derivative led to a *global* maximum at z^*=1 in the present analysis, although this boundary condition may also depict a *local* maximum/minimum, or a horizontal constant profile. The nonlinear boundary value problem thus needs a refining of this boundary condition to better represent the evolution of IJ along the whole $z^{\S}$ axis. The results already obtained for $z^{\S}\rightarrow 0$ are, however, promising, and induce further studies on the theme.

5. EFFECT OF THE NUMBER OF PARCELS OF THE TAYLOR SERIES

Usually, if a small number of parcels is used in a Taylor series, the obtained results may be affected by an observable error, which tend to be smaller for higher number of parcels. In the present study the values of the control parameters are very relevant to define the behavior of the profile of n at the interface, and by increasing the number of parcels of the Taylor series the difference between successive profiles may also increase. To show the effect of the number of parcels, Figs. 9 and 10 present respectively the evolution of n-profiles and of the difference between successive n-profiles for the agitation state given by A_1=0.6, IJ_1=7, Sh=0.1, when changing the number of parcels. An asymptotically superposing behavior of the n-profiles is observed by increasing the number of parcels, while the difference between successive profiles decreases. Related profiles for this condition also naturally show asymptotic behaviors, as shown by the profiles of the derivative of n in Fig. 11.

The evolution of the profiles for other agitation levels (other values of the control parameters) may differ of those shown in Figs. 9, 10 and 11. To clarify this aspect, Figs. 12, 13, and 14 were built for the agitation state characterized by the parameters A_1=0.6, IJ_1=7, Sh=0.49, already discussed in Fig. 6b. Figure 12 shows that the profiles have a visual closer evolution for the different number of parcels, varied between 10 and 24 parcels.

Figure 13 shows that the differences between two successive profiles may have a nonlinear behavior. For this combination of parameters, a "decreasing-increasing-decreasing" sequence is observed for the differences. Figures 10 and 13 indicate that more studies on n profile's details and control parameters will be positive for this field of knowledge.

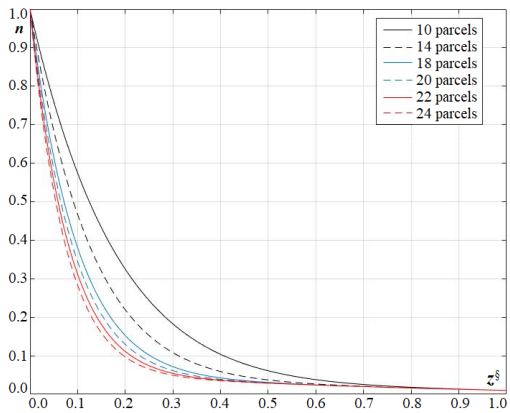

Fig. 9. Effect of number of parcels of the Taylor series on the *n*-profile for A_1=0.6, IJ_1=7, Sh=0.1.

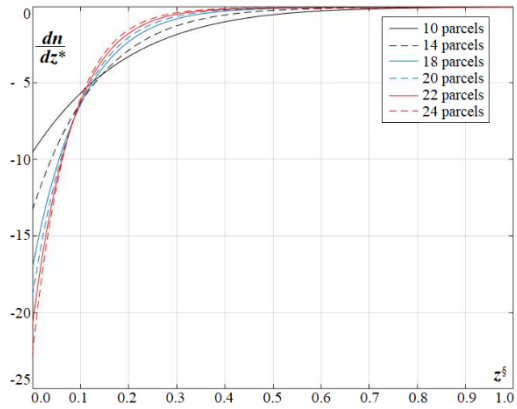

Fig. 11. Effect of number of parcels on the profile of d*n*/d*z for A_1=0.6, IJ_1=7, Sh=0.1.**

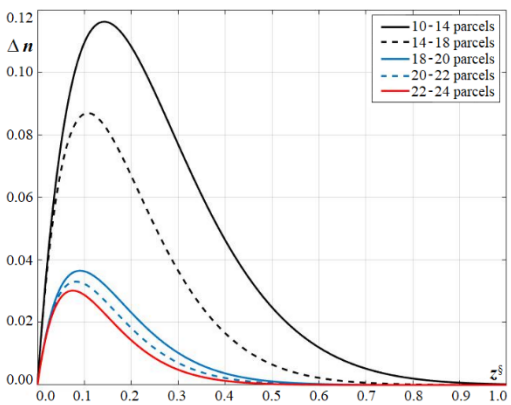

Fig. 10. Differences between successive *n*-profiles for A_1=0.6, IJ_1=7, Sh=0.1.

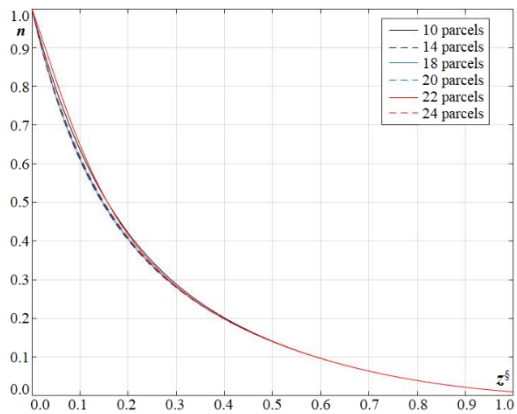

Fig. 12. Effect of number of parcels of the Taylor series on the *n*-profile for A_1=0.6, IJ_1=7, Sh=0.49.

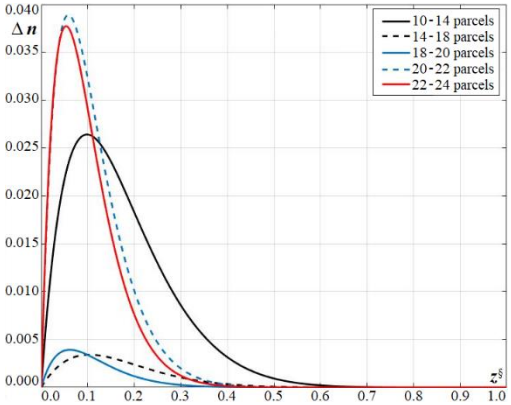

Fig. 13. Differences between successive *n*-profiles for A_1=0.6, IJ_1=7, *Sh*=0.49.

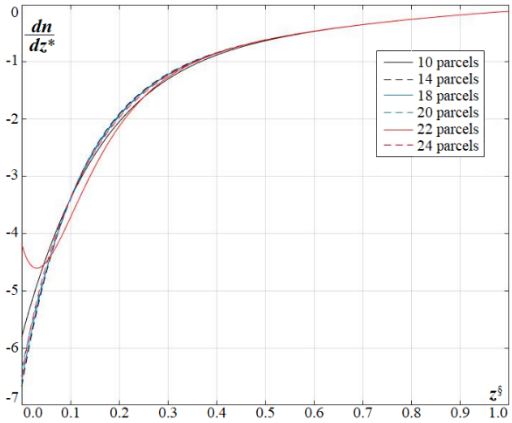

Fig. 14. Effect of number of parcels on the profile of d*n*/dz* for A_1=0.6, IJ_1=7, *Sh*=0.49.

Figure 14 shows the derivatives of the *n* profiles for A_1=0.6, IJ_1=7, *Sh*=0.49, evidencing the evolution to a minimum for the derivative, as mentioned in Fig.6b. Figures 11 and 14 also suggest more studies on the details of the interface *n* profiles in relation to the control parameters.

As described, the use of Taylor series has the "disadvantage" of being constituted of an infinite number of parcels, being thus unavoidable to impose a truncation, and, as a consequence, to introduce the related truncation error. A further characteristic of the method is that the convergence of the series to final stable profiles depends on the values of the control parameters. A tool that quantifies the number of parcels having a predefined residual error and the values of the control parameters is still not available, so that each combination of values must be tested. Evidently future studies may be directed to evaluate these aspects, and to allow quicker applications.

It must also be noted that only two positions were used in the present study to apply the six physically based boundary conditions (three second order differential equations). Although adequate for the present study, these conditions are not definitive. Different physically justified boundary conditions may be proposed and used, in the sense of improve the obtained profiles. This possibility shows that the method is very open to contributions, and that they may expand its application potential.

6. CONCLUSIONS

The Random Square Waves method (RSW) was described and applied to obtain mean profiles of variables related to turbulent mass transfer across air/water interfaces in the scalar boundary layer region. The main focus was the mean concentration profile, followed by the turbulent mass flux profiles, and reduction function profiles. Although involving a large number of parcels in its general form (Eq. 10), the RSW method allows defining a proper closed set of equations for the one-dimensional transport of scalar properties. The method thus surpasses the closure problem of statistical turbulence, meaning that supplementary models (Boussinesq hypothesis, for example) or auxiliary equations are not necessary (*ad hoc* approximations for the turbulent viscosity, for example).

Considering the use of Taylor series to obtain the profiles for the concentration and related statistical variables, following positive aspects are evidenced:

i) – The Taylor series allow to adequately treat the nonlinear boundary condition problem.

ii) – The series may be centered in convenient points in the domain of calculation. In the present study they were centered at z*=1.

iii) – Truncations of the infinite series are needed, allowing to adequately recalculate coefficients to express the boundary conditions of the problem.

iv) – The coefficients can be theoretically calculated through symbolic codes, like symbolic MATLAB ®.

The results indicate that the calculated profiles follow most features of observed profiles of the literature. It was shown that the boundary layer mass transfer problem is linked to three RSW functions: i) the partition function *n* (which corresponds to the normalized concentration profile) ii) the reduction function *a*=1-*A*, and iii) the turbulent mass transfer *IJ*, thus needing three equations to be solved. The Taylor series were used to represent each of the three mentioned functions. The adequate number of terms of the Taylor series in the present study were 24 for *n*, 24 for *A* and 25 for *IJ*, centered at the immersed border of the region of variation of the mean concentration (the aforementioned position *z**=1.0). A set of six physically justified boundary conditions for the different variables (*n*, *A*, and *IJ*) was applied, a procedure not followed in previous studies on the theme. The six conditions are needed because the RSW method generated three second order differential equations for the one-dimensional mass transfer. The profiles were conditioned by three nondimensional control parameters, two of them (A_1 and IJ_1) were restricted to the interval [0,1], and the third given by the modified Sherwood number. These control parameters are a consequence of the RSW method, thus not existing in previous studies that used other models or tools to quantify statistical parameters of the interfacial region. It was observed

that the maximum modified Sherwood number appliable to an agitation condition depends on the value of the two remaining control parameters, a condition that suggests further studies on this dependence.

The obtained normalized concentration profiles followed the features observed in experimental profiles of the literature. Considering the sub superficial conditions very close to the interface for slightly soluble gases, and which are related to the form of the profiles, the present results indicate that it is possible to have both behaviors for the *n* profiles: i) solutions with the maximum slope of the profile (derivative or gradient in relation to the axis normal to the surface) at the interface, in agreement with most of the studies of the literature, and ii) solutions with the maximum slope located at positions below the interface, previously considered for laminar flows in the literature, but also measured in turbulent flows and justified as methodologic imagery distortions at the interface. This new theoretical result indicates that measured smaller slopes at the interface may be not only due to distortions of optical measurement methods, but also partially represent the physical phenomenon itself, and that this condition may be dependent on the agitation level of the surface. In this sense, experimental and numerical procedures that impose maximum slope at the interface may need adjustments. Further studies to better determine the characteristics of *n* profiles at the air-water interface are very welcomed.

Some eventual "disadvantages" of using the Taylor series were also mentioned, like the truncation errors that follow from the truncations needed for practical purposes. There is still no tool to predict the number of parcels needed to attain a predefined residual error, a quantification that depends on the predefined error itself, and also on the agitation conditions given by the combination of the three control parameters. Further, the propagation of errors with the number of parcels is also an interesting aspect for future studies.

Considering the procedures described in this study, the RSW method is easy to implement, being an adequate tool to study different aspects of turbulent scalar boundary layers. The obtained results suggest its use to analyze details of statistical profiles of relevant variables in the region very near to the gas-liquid interface. The present results also show that further studies on aspects of the method that were still not covered are very welcomed, like:

i) Different boundary conditions applied at different points of the domain of calculation of the nonlinear boundary value problem.

ii) Experimental measurements of the profiles of the variables a=1-A and IJ in the boundary layer region close to the interface, which are still very rare in the literature.

iii) A better reproduction of the "growth and fall" behaviors of the A and IJ profiles, which may also depend on the definitions of boundary conditions.

iv) A tool that quantifies the number of parcels of the Taylor series necessary to attain a predefined residual error.

ACKNOWLEDGEMENTS

To CNPq, Brazil, for the scholarship of the second author, process 307105/2015-6. To Prof. Ingo Schulz for relevant initial advices and financial support T.I.M *bó* 04031-928-2005 through him for the first author; and to Prof. Janka Neuwiem for decisive advices in the final part, and financial support: K.I.E. *lce* 20061-936-2021 through her for the first author.

REFERENCES

Asano, K. (2006). *Mass Transfer: From Fundamentals to Modern Industrial Applications*. Wiley-VCH Verlag GmbH & Co. KGaA, Weinheim Germany.

Bennett, J. P. and R. E. Rathbun (1971). *Reaeration in Open-Channel Flow.* US Department of the Interior, Geological Survey.

Bongo, D., N. D. Clarisse and J. Y. Champagne (2021). Effect of an oscillating grid on hydrodynamics and gas-liquid mass transfer in an aquarium. *Fluid Mechanics* 7(1), 9-16.

Boyadjiev, C. and P. Mitev (1977). On the concentration boundary layer theory at a moving interface. *The Chemical Engineering Journal* 14(3), 225-228.

Brumley, B. (1984). Turbulence measurements near the free surface in stirred grid experiments. In W. Brutsaert and G. H. Jirka (Eds), *Gas Transfer at Water Surfaces. Water Science and Technology Library*, 2, 83-92. Springer, Dordrecht.

Brumley, B; G.H. Jirka (1987). Near-surface turbulence in a grid-stirred tank. *Journal of Fluid Mechanics*, 183, 235-263.

Brumley, B. and G. H. Jirka (1988). Air-water transfer of slightly soluble gases: turbulence, interfacial processes and conceptual models. *Physico-Chemical Hydrodynamics* 10(3), 295-319.

Chu, C. R. and G. H. Jirka (1992). Turbulent gas flux measurements below the air-water interface of a grid-stirred tank. *International Journal of Heat and Mass Transfer* 35(8), 1957-1968.

Cunha, A. C., D. C. Brito, H. F. A. Cunha and H. E. Schulz (2011). Dam Effect on Stream Reaeration Evaluated with the Qual 2kw Model: Case Study of the Araguari River, Amazon Region, Amapá State/Brazil. In C. Bilibio, O. Hensel and J. Selbach (Eds.), *Sustainable Water Management in the Tropics and Subtropics-and Case Studies in Brazil.* 1ed.Kassel: Unikassel, 2, 153-177.

Danckwerts, P. V. (1951). Significance of liquid-film coefficients in gas absorption. *Industrial & Engineering Chemistry* 43, 1460-1467.

Donelan, M. A., W. M. Drennan., E. S. Saltzman and R. Wanninkhof (2002). Gas transfer at water surfaces. *Geophysical Monograph Series* 127.American Geophysical Union.

EPA Environmental Protection Agency (1995). QUAL2E *Windows Interface User's Manual*, EPA-823-95-003, Office of Water, U.S.A.

Flagiello, D., A. Parisi, A. Lancia and F. Di Natale (2021). A review on gas-liquid mass transfer coefficients in packed-bed columns. *Chem Engineering* 43(5), 1-29.

Friedl, F. (2013) *Investigating the Transfer of Oxygen at the Wavy Air-Water Interface Under Wind-Induced Turbulence*. Ph. D. Thesis, University of Heidelberg, Heidelberg, Germany.

Gonçalves, B. B. (2014). *Detailing the 1-D solution of the RSW Method Taking a Constant Reduction Function for the Turbulent Interfacial Scalar Transport* (in Portuguese). M. Sc. Thesis, University of São Paulo, Brazil.

Gonçalves, B. B. and H. E. Schulz (2013) One-dimen-sional turbulent mass transfer at air-water inter-faces: details of discontinuities of derivatives using the RSW method. *WIT Transactions on Engineering Sciences* 79, 365-376.

Gulliver, J. S. (1991). Introduction to air-water mass transfer. In *Proceedings of the 2nd International Symposium on Gas Transfer at Water Surfaces*, Minneapolis, USA, ASCE.

Herlina, H. (2005). *Gas Transfer at the Air-Water Inter-Face in A Turbulent Flow Environment.* Ph. D. Thesis, University of Karlsruhe, Karlsruhe, Germany.

Herlina, H. and G. H. Jirka (2004). Application of LIF to investigate gas transfer near the air-water interface in a grid-stirred tank. *Experiments in Fluids* 37(3), 341-349.

Herlina, H. and G. H. Jirka (2007). Experiments on gas transfer at the air–water interface induced by oscillating grid turbulence. *Journal of Fluid Mechanics* 594, 183-208.

Herlina, H. and J. G. Wissink (2019). Simulation of air–water interfacial mass transfer driven by high-intensity isotropic turbulence. *Journal of Fluid Mechanics* 860, 419-440.

Higbie, R. (1935). The rate of absorption of a pure gas into a still liquid during short periods of exposure. *Transactions of the Amerixan Institute of Chemical Engineers* 35, 36-60.

Hinze, J. O. (1959). *Turbulence*. McGraw Hill, UK.

Hunt, J. C. R. (1984). Turbulence structure and tur-bulent diffusion near gas-liquid interfaces. In W. Brutsaert and G. H. Jirka (Eds.), *Gas Transfer at Water Surfaces. Water Science and Technology Library*, 2, 67-82. Springer, Dordrecht.

Jähne, B. (2020). Struktur und chaos: kleinskalige austauschprozesse zwischen atmosphäre und meer. In J. Funke and M. Wink (eds.), *Entwicklung Wie aus Prozessen Strukturen warden*. Heidelberger Jahrbücher Online HDJBO (5), 195-218,

Jähne, B. and H. Haussecker (1998). Air-water gas exchange. *Annual Review of Fluid Mechanics* 30(1), 443-468.

Janzen, J. G. (2006). *Gas Transfer Near the Air-Water Interface in Oscillating-Grid Tanks and Properties of Isotropic Turbulent Flows* (in Portuguese). M. Sc. Thesis, University of São Paulo, Brazil.

Janzen, J. G., H. Herlina, G. H. Jirka, H. E. Schulz and J. S. Gulliver (2010a). Estimation of mass transfer velocity based on measured turbulence parameters. *AIChE Journal* 56(8), 2005-2017.

Janzen, J. G., H. E. Schulz and G. H. Jirka (2010b). Turbulent gas flux measurements near the air–water interface in an oscillating-grid tank. In S. Komori, W. McGillis and R. Kurose (Eds.), *Gas Transfer at Water Surfaces*, 65-77, Kyoto, Japan.

Jorgensen, S. E. and M. J. Gromiec (1989). Mathematical submodels in water quality systems: Reaeration. *Developments in Environmental Modelling* 14, 33-64.

Lacassagne, T., M. El-Hajem, F. Morge, S. Simoëns and J. Y. Champagne (2017a). Study of gas liquid mass transfer in a grid stirred tank. *Oil & Gas Science and Technology* 72(7), 1-16.

Lacassagne, T., M. El Hajem, S. Simoëns and J. Y. Champagne (2017b). In *Experimental study of gas-liquid mass transfer enhanced by oscillating grid turbulence*, 23ème Congrès Français de Mécanique, Lille.

Lamont, J. C. and D. S. Scott (1970). An eddy cell model of mass transfer into the surface of a turbulent liquid. *AIChE Journal* 16(4), 513-519.

Lavín, F. A. L. (2020). *Theoretical Study of the Turbulent Mass Transfer Through Free Surfaces Using Random Square Waves*. Ph. D. Thesis, University of São Paulo, Brazil.

Lavín, F. A. L. and H. E. Schulz (2019). Mass transfer through free surface boundary layers using a statistical approach. *WIT Transactions on Engineering Sciences* 123, 77-88.

Lewis, W. K. and W. G. Whitman (1924). Principles of gas absorption. *Industrial and Engineering Chemistry* 16, 1215-1220.

Lopes Jr., G. B. (2012). *Organizing Statistical Equa-Tions of Mass Transfer in Turbulent Processes*. M. Sc. Thesis, University of São Paulo, Brazil.

Luk, S. and Y. H. Lee (1986). Mass transfer in eddies close to air-water interface. *AIChE Journal* 32(9), 1546-1554.

Mackinnon, P. A.; T. Elliot, Y. Q. Zhao, J. L. Murphy and R. M. Kalin (2002). Evaluation of

a novel technique for measuring reaeration in rivers. In C. A. Brebbia and P. Zannetti (Eds.), *Development and Application of Computer Techniques to Environmental Studies*, WIT Press, UK.

Magnaudet, J. and I. Calmet (2006). Turbulent mass transfer through a flat shear-free surface. *Journal of Fluid Mechanics* 553, 155-185.

McCorquodale, M. and R. J. Munro (2017). Experimental study of oscillating-grid turbulence interacting with a solid boundary. *Journal of Fluid Mechanics* 813, 768-798.

McCready, M. J., E. Vassiliadou and T. J. Hanratty (1986). Computer simulation of turbulent mass transfer at a mobile interface. *AIChE Journal* 32(7), 1108-1115.

Rodi, W. (2000). *Turbulence Models and Their Application in Hydraulics A State-of-the-Art Review*. IAHR, International Association of Hydraulic Research, Monograph Series.

Schulz, H. E. (1985). *Investigating the Reoxigenation Mechanism of Flowing Waters and Its Relation with the Turbulence Level Close to the Surface - 1.* M. Sc. Thesis, University of São Paulo, Brazil.

Schulz, H. E. and S. A. G. Schulz (1991). Modelling below surface characteristics in water reaeration. In L. C. Wrobel and C. A. Brebbia (Eds.), *Water Pollution: Modelling, Measuring and Prediction*, 441-454. Springer, Dordrecht.

Schulz, H. E. and J. G. Janzen (2009). Concentration fields near air-water interfaces during interfacial mass transport: oxygen transport and random square wave analysis. *Brazilian Journal of Chemical Engineering* 26(3), 527-536.

Schulz, H. E., A. L. A. Simões and J. G. Janzen (2010). Statistical approximations in gas-liquid mass transfer. In S. Komori, W. McGillisa and R. Kurose (Eds.), *Gas Transfer at Water Surfaces*, 208-221, Kyoto, Japan.

Schulz, H. E., G. B. Lopes Jr, A. L. A. Simões and R. J. Lobosco (2011). One dimensional turbulent transfer using random square waves–scalar/ velocity and velocity/velocity interactions. In H. E. Schulz., A. L. A. Simões and R. J. Lobosco (Eds.), *Hydrodynamics-Advanced Topics*, 3-34, Intech.

Schulz, H. E. and B. B. Gonçalves (2015) Solutions of scalar mean profiles close to gas-liquid interfaces under turbulent free slip motion. *WIT Transactions on Engineering Sciences* 89, 33-44.

Schulz, H. E.; F. A. L. Lavín and B. B. Gonçalves (2018). Turbulence aspects of mass transfer in the thin interfacial region of the concentration boundary layer in gas–liquid systems. *International Journal of Computational Methods and Experimental Measurements* 6(1), 186-197.

Schulz, H. E. (2022). Differential equation for turbulence power losses and energy spectra based on consolidated empirical results. *Journal of Applied Fluid Mechanics* 15 (4), 959-972.

Tamburrino, A. and J. S. Gulliver (2002). Free-surface turbulence and mass transfer in a channel flow. *AIChE Journal* 48(12), 2732-2743.

Theofanous, T. G. (1984). Conceptual models of gas exchange. In W. Brutsaert and G. H. Jirka (Eds.), *Gas Transfer at Water Surfaces. Water Science and Technology Library*, 2, 271-281. Springer, Dordrecht.

Toor, H. L. and J. M. Marchello (1958) Film-penetration model for mass and heat transfer. *AIChE Journal* (4), 97-101.

Turney, D. E. and S. Banerjee (2013). Air–water gas transfer and near-surface motions. *Journal of Fluid Mechanics* 733, 588-624.

Wanninkhof, R., W. E. Asher, D. T. Ho, C. Sweeney and W. R. McGillis (2009). Advances in quantifying air-sea gas exchange and environmental forcing. *Annual Review of Marine Sciences* 1, 213-244.